NREL GOES Reference Document

Michael J. Foster,[1] Yue Li,[1] and Andrew K. Heidinger[2]

1 Space Science and Engineering Center, University of Wisconsin – Madison
2 NOAA/NESDIS/GeoXO

NREL Technical Monitor: Yu Xie

NREL is a national laboratory of the U.S. Department of Energy
Office of Energy Efficiency & Renewable Energy
Operated by the Alliance for Sustainable Energy, LLC

This report is available at no cost from the National Renewable Energy Laboratory (NREL) at www.nrel.gov/publications.

Contract No. DE-AC36-08GO28308

Subcontract Report
NREL/SR-5D00-89513
August 2024

NREL GOES Reference Document

Michael J. Foster,[1] Yue Li,[1] and Andrew K. Heidinger[2]

1 Space Science and Engineering Center, University of Wisconsin – Madison
2 NOAA/NESDIS/GeoXO

NREL Technical Monitor: Yu Xie

Suggested Citation
Foster, Michael J., Yue Li, and Andrew K. Heidinger. 2024. *NREL GOES Reference Document*. Golden, CO: National Renewable Energy Laboratory. NREL/SR-5D00-89513. https://www.nrel.gov/docs/fy24osti/89513.pdf.

NREL is a national laboratory of the U.S. Department of Energy
Office of Energy Efficiency & Renewable Energy
Operated by the Alliance for Sustainable Energy, LLC

This report is available at no cost from the National Renewable Energy Laboratory (NREL) at www.nrel.gov/publications.

Contract No. DE-AC36-08GO28308

Subcontract Report
NREL/SR-5D00-89513
August 2024

National Renewable Energy Laboratory
15013 Denver West Parkway
Golden, CO 80401
303-275-3000 • www.nrel.gov

NOTICE

This work was authored [in part] by the National Renewable Energy Laboratory, operated by Alliance for Sustainable Energy, LLC, for the U.S. Department of Energy (DOE) under Contract No. DE-AC36-08GO28308. This work was supported by the U.S. Department of Energy Office of Energy Efficiency and Renewable Energy Solar Energy Technologies Office. The views expressed herein do not necessarily represent the views of the DOE or the U.S. Government.

Cover Photos by Dennis Schroeder: (clockwise, left to right) NREL 51934, NREL 45897, NREL 42160, NREL 45891, NREL 48097, NREL 46526.

REVISION HISTORY

Rev.	Author	Description	Date
1	Michael Foster and Leanne Avila, CIMSS	Original document – put together from excerpts from algorithm ATBDs and the PATMOS-x User Guide	09/17/2018
2	Michael Foster, CIMSS	Updated to reflect operation with GOES-R	09/20/2019
3	Yue Li and Michael Foster, CIMSS	Revised to a concise version and reflect algorithm updates and GOES-17 LHP issues	01/31/2024

List of Acronyms

ABI	Advanced Baseline Imager
ACHA	AWG Cloud Height Algorithm
AHI	Advanced Himawari Imager
AMI	Advanced Meteorological Imager
AMV	Atmospheric Motion Vector
ATBD	Algorithm Theoretical Basis Documents
AVHRR	Advanced Very High Resolution Radiometer
AWG	(GOES-R) Algorithm Working Group
CALIOP	Cloud-Aerosol Lidar with Orthogonal Polarization
CALIPSO	Cloud-Aerosol Lidar and Infrared Pathfinder Satellite Observations
CASPR	Cloud and Surface Parameter Retrieval
CEM	cloud emissivity
CFSR	Climate Forecast System Reanalysis
CIMSS	Cooperative Institute for Meteorological Satellite Studies
CLAVR-x	Clouds from AVHRR Extended
COD	cloud optical depth
CPS	cloud particle size
CRE	cloud particle radius
CTT	cloud top temperature
DCOMP	Daytime Cloud Optical and Microphysical Properties
ECM	Enterprise Cloud Mask
EUMETSAT	European Organisation for the Exploitation of Meteorological Satellites
FY	FengYun
GOES	Geostationary Operational Environmental Satellites
IWP	ice water path
LHP	loop heat pipe
LUT	lookup table
LWP	liquid water path
MetOp	Meteorological Operational satellite
MODIS	Moderate Resolution Imaging Spectroradiometer
MTSAT	Multi-functional Transport Satellite
NASA	National Aeronautics and Space Administration
NCEP	National Centers for Environmental Prediction
NESDIS	National Environmental Satellite, Data, and Information Service
NOAA	National Oceanic and Atmospheric Administration
NREL	National Renewable Energy Laboratory
NSRDB	National Solar Radiation Database
NWP	numerical weather prediction
PATMOS-x	Pathfinder Atmospheres Extended
RTM	Radiative Transfer Model
SEVIRI	Spinning Enhanced Visible and InfraRed Imager
1D-VAR	one-dimensional variational
VIIRS	Visible Infrared Imaging Radiometer Suite

Table of Contents

List of Figures

List of Tables

1 Introduction

The purpose of this document is to create a single reference document representing abridged versions of the Pathfinder Atmospheres Extended (PATMOS-x) Algorithm Theoretical Basis Documents (ATBDs) specifically relevant to Geostationary Operational Environmental Satellites (GOES)-16, GOES-17, and GOES-18 processing. This document has been compiled from several ATBDs:

- *ABI Cloud Mask*[1]
- *Enterprise AWG Cloud Height Algorithm (ACHA)*[2]
- *Daytime Cloud Optical and Microphysical Properties (DCOMP)*[3]
- *The Clouds from AVHRR Extended (CLAVR-x) User's Guide*.[4]

These documents can also be found at:

- https://cimss.ssec.wisc.edu/patmosx/documentation.html
- https://cimss.ssec.wisc.edu/clavrx/documentation/.

Besides, additional ATBD references can be found at the GOES-R document section at https://www.goes-r.gov/resources/docs.html

As of January 2024, GOES-16, GOES-17, and GOES-18 are the three currently operating satellites in the GOES-R series. GOES-16 launched in November 2016 and became the operational GOES-East satellite in December 2017. GOES-17 became the operational GOES-West satellite in February 2019 but was reported to have a loop heat pipe (LHP) issue. This significantly impacted its performance and will be discussed later. GOES-T launched on March 1, 2022, and was renamed to GOES-18 on March 14, 2022. GOES-18 became operational service as GOES-West on Jan. 4, 2023.

The retrieval algorithms in this document were developed to work with many different sensors, depending on the specific channels available. For GOES-16, GOES-17, and GOES-18, the same channels settings are applied, except for GOES-17 during the LHP event when certain affected channels needed to be shut off for the cloud height algorithm. The GOES-R series provides significant improvements in spatial, spectral, and temporal information. The current scanning mode provides 5-minute contiguous U.S. and 10-minute full disk imagery at a 2-km resolution. Product examples for these satellites are included at the end of this document for comparison with previous GOES imagers. More information on the additional channels and resolutions of the Advanced Baseline Imager (ABI) sensor can be found at https://www.goes-r.gov/spacesegment/ABI-tech-summary.html.

[1] See https://docs.google.com/document/d/18e67VUspdlTY_pn5mBYrTHSJDew0d2nmk8BylijuK9s/edit
[2] See https://docs.google.com/document/d/1m2SatR91WIJcaAZweongcFCb6Wsx_xnRUcZxp94gXHk/edit
[3] See https://www.star.nesdis.noaa.gov/goesr/documents/ATBDs/Enterprise/ATBD_Enterprise_Daytime_Cloud_Optical_and_Microphysical_Properties(DCOMP)_v1.2_2020-10-09.pdf
[4] See https://docs.google.com/document/d/1NHuKBJr23i1k0ysihoyThg32e44l4CoDe5CjWydn0JI/edit.

2 Introduction to CLAVR-x/PATMOS-x

CLAVR-x is a processing system developed at the National Oceanic and Atmospheric Association (NOAA)/National Environmental Satellite, Data, and Information Service (NESDIS) and the University of Wisconsin Cooperative Institute for Meteorological Satellite Studies (CIMSS) for generating quantitative cloud products in real time from the Advanced Very High Resolution Radiometer (AVHRR). CLAVR-x become operational in NESDIS in 2002 and was significantly updated in 2006 after the launch of Meteorological Operational satellite (MetOP)-A. In 2013, CLAVR-x was updated again to support the generation of higher-spatial-resolution output for the National Centers for Environmental Prediction (NCEP) and incorporated many algorithm improvements from the GOES-R AWG effort. CLAVR-x algorithms are now designed to operate in several processing systems to support NESDIS's needs for cloud products in other applications and sensors. Currently, CLAVR-x supports many sensors, including the Visible Infrared Imaging Radiometer Suite (VIIRS); the Moderate Resolution Imaging Spectroradiometer (MODIS); AVHRR (NOAA-8 through NOAA-19); GOES-8 through GOES-15; ABI (GOES-16, GOES-17, and GOES-18); the Spinning Enhanced Visible and InfraRed Imager (SEVIRI); the Advanced Himawari Imager (AHI) (Himawari 8 and 9); the Communication, Ocean and Meteorological Satellite (COMS); the Advanced Meteorological Imager (AMI); the Multi-functional Transport Satellite (MTSAT); MetOp-A, MetOp-B, and MetOp-C; and FengYun (FY)-2D/E, FY-3D, and FY-4A.

The CLAVR-x system has also evolved into a climate processing system called the Pathfinder Atmospheres Extended (PATMOS-x) system. PATMOS-x uses the same algorithms as CLAVR-x, but it is run using different sources of ancillary data to generate a more consistent record suitable for climate applications. A simple way to think of this relationship is that CLAVR-x is used for algorithm development and real-time operational products, whereas PATMOS-x is used for long-term, stable, climate records. The cloud products derived from the GOES sensors and used for the National Renewable Energy Laboratory (NREL) National Solar Radiation Database (NSRDB) are run using PATMOS-x. Therefore, throughout most of this document, we will refer to the GOES processing system as PATMOS-x, though note that CLAVR-x and PATMOS-x are essentially interchangeable.

2.1 Description of the PATMOS-x Processing System

The PATMOS-x system consists of several executables. The main executable is called clavrxorb, and it operates on the Level 1b data and generates Level 2 products. The primary cloud products are as follows:

- Cloud mask
- Cloud type/phase
- Cloud top temperature/height/pressure (ACHA)
- Daytime cloud optical and microphysical properties (DCOMP)
- Cloud base temperature/height/pressure
- Cloud cover layer.

PATMOS-x runs physical algorithms and therefore uses significant amounts of ancillary data to specify the atmospheric and surface conditions. The algorithm is designed to run on segments of

data to save memory, where a segment consists of multiple scan lines. For details, see the complete list of ATBDs in Section 1.

2.2 Level 1b Input: GOES-R Imager

PATMOS-x processes can process both McIDAS "area" files and NetCDF format for GOES-R generation (GOES-16, GOES-17, and GOES-18). For NSRDB delivery, the NetCDF format is processed by PATMOS-x. The naming convention for these files is: OR_*Sensor*-L1b-*ScanArea_ScanMode_Satname*_s*YYYYDOYHHMMSEC*_e*YYYYDOYHHMMSEC*_c*YYYYDOYHHMMSEC*.nc, where s = start, e = end, and c = created.

Example file name:

OR_ABI-L1b-RadF_M6C16_G16_s20191202040258_e20191202049578_c20191202050029.nc

2.3 Level 2 Output: Level 2 File Contents

The contents of the Level 2 file are defined by the user through the variable name in the level2_list file. Table A1 lists all variables that are included in the Level 2 files delivered to NREL.

2.4 Algorithms

2.4.1 Cloud Detection (ECM)

Cloud detection is the process of separating cloudy from clear pixels. It always involves assumptions of the radiometric characteristics of the clear and/or cloudy state and looking for departures from them. Spectral and spatial tests are used to look for clouds by identifying pixels that do not exhibit the expected behavior of the clear-sky state. The Enterprise Cloud Mask (ECM) algorithm makes extensive use of information from numerical weather prediction (NWP) fields, coupled with a Radiative Transfer Model (RTM), to generate the expected clear-sky state for the spectral tests. This approach has also been adopted by the European Organisation for the Exploitation of Meteorological Satellites (EUMETSAT) (Dybbroe, Karlsson, and Thoss 2005a; 2005b). Although the current NWP data often have errors in some critical fields, such as the surface temperature over land, they provide needed and useful information. Each test is applied to each pixel, resulting in a cloud/no cloud score, which is then used to decide whether a pixel is cloudy or clear. The spectral tests are categorized by those that use infrared, shortwave infrared, and solar-reflectance channels. All applicable tests are used to construct the ECM using the naïve Bayesian approach, which is an artificial intelligence/machine learning technique. In the full or classical Bayesian approach, the probability of a given passive satellite pixel being cloudy for a set of features (F) is given by $P(C_{yes}|F)$, which is defined as:

$$P(C_{yes} \mid F) = \frac{P(C_{yes})P(F \mid C_{yes})}{P(F)} \quad (1)$$

where $P(C_{yes})$ is the prior probability of any pixel being cloudy without any knowledge of F, and $P(F)$ is the probability of the existence of the pixel's set of features (F). $P(F|C_{yes})$ is the probability of the existence of the pixel's set of features for the cloudy pixels. The components in

the feature set *F* are referred to as the cloud mask classifiers, and the particular features employed in this approach involve a number of tests, including visible and infrared channels and NWP, for different surface types. The Bayesian context, $P(C_{yes}|F)$, is referred to as the posterior probability.

For the ABI, an analysis of colocated GOES-16/ABI and Cloud-Aerosol Lidar and Infrared Pathfinder Satellite Observations (CALIPSO)/ Cloud-Aerosol Lidar with Orthogonal Polarization (CALIOP) observations was used to automatically derive the Bayesian classifiers globally. This methodology has been extended to all the sensors supported by PATMOS-x. An important part in the development of ECM is the use of CALIPSO observations to help define the classifiers. Because CALIPSO provides one of the most unambiguous and direct measures of the presence of the highest cloud layers (i.e., those also observed by the passive sensors), it has been used to help understand the behavior of each cloud mask test for clear and cloudy pixels. Although many cloud masks have used RTM simulations to set cloud detection thresholds (i.e., CASPR), the goal of the ECM is to use the availability of pixel-level clear-sky information to derive new cloud mask metrics that maximize the separation of cloudy and clear pixels. The main advantage of using an observationally based approach (collocation of CALIPSO and passive sensor test data) to define thresholds is that simulations might not capture the true variability present in real scenes. The ECM allows for threshold modification when warranted.

The artificial intelligence/machine learning technique with the National Aeronautics and Space Administration (NASA)/CALIOP training data provides a consistent basis for the ECM on all sensors. ECM is probabilistic but still generates a binary and four-level mask with individual test bits. ECM comprises individual lookup tables (LUTs) that can be 1D, 2D, or 3D. Each LUT is computed separately for each of seven ECM surface types. Determining which classifiers to include in ECM is a major decision. For ABI, there were roughly 50 candidate classifiers based on different mixtures of thermal, solar, RTM, and other metrics. Like most machine learning approaches, we employ an optimization approach to select the classifiers, and it is performed over each of the seven ECM surface types. This occasionally results in classifiers not being used for some surface types. Sequential optimization greatly improves ECM performance and reduces harmful inter-classifier correlation. A sequential optimization approach works by finding the first classifier with the best individual performance and then selecting the next classifier that most improves the performance in conjunction with the first. This is repeated until no more improvement is found.

As a lidar with an inherent vertical resolution of 30 m, CALIPSO can detect clouds with opacities and spatial scales far exceeding the capabilities of passive visible/infrared sensors such as ABI. To use CALIPSO to determine meaningful thresholds for the passive detection of clear and cloudy conditions, filtering is required to attempt to make the CALIPSO detection comparable to the performance expected from the passive observing system. In this analysis, we ignored all CALIPSO results that had cloud fractions between 0.1 and 0.9. Here, cloud fraction is computed using results from all lidar fields of view that fell within each ABI pixel. The purpose of this filter is to restrict the analysis to CALIPSO data that are uniform over the spatial scales of the coarser ABI pixels. In addition, a threshold of 0.1 was applied to the CALIPSO emissivity in an attempt to remove from consideration any pixels with very low optical depths that would fall below the detection capabilities of the channels on the passive sensors. Here, CALIPSO emissivity is derived based on the following procedure: Using the method described in Heidinger

and Pavolonis (2009), the temperature of the highest cloud layer observed by CALIPSO is used in conjunction with the 11-µm clear radiance calculation and 11-µm ABI observations to compute an 11-µm cloud emissivity. This value represents the emissivity that a cloud must have if it existed at the level measured by CALIPSO with the observations measured by the passive sensor (i.e., ABI). This is hereafter referred to as the CALIPSO emissivity.

The other major type of test in the ECM is the restoral test. The restoral tests are separated into tests that "restore" probably cloudy pixels to clear pixels and tests that "restore" cloudy pixels to probably cloudy pixels. As defined, the effect of these restoral corrections is to provide a conservative estimate on cloudiness (i.e., minimize false alarms in the ECM).

Other than cloud mask and probability, a retrieval uncertainty is reported, and the ability to report uncertainties is a critical component of this approach. Relative to CALIPSO, a recent GOES-16 product review shows a probability of correct detection of roughly 90% overall and a similar performance over snow/ice surface where retrieval uncertainty is usually larger. This demonstrates the stability and consistency of ABI cloud mask products.

2.4.1.1 ECM Mitigation for GOES-17 Loop Heat Pipe Issue

GOES-17 was moved into operational service as GOES-West on Feb. 12, 2019; however, there is a well-known issue with the GOES-17 ABI detector cooling system. The LHP system, which cools the ABI detectors, does not adequately maintain the optimal temperatures. During nighttime, before and after both equinoxes, the sun heats up several of the ABI infrared detectors and degrades the imagery to the point of being unusable. Mitigation for ECM uses the focal plane temperature of each channel. If the focal plane temperature reaches the designated threshold for a given channel, the ECM tests that use those channels are not used; ECM will still run, but the product is marked as degraded, and channel noise and striping are expected in the cloud mask. Figure 1 shows the cloud mask during an LHP event; as shown, most noise is in the probably clear/cloudy regions.

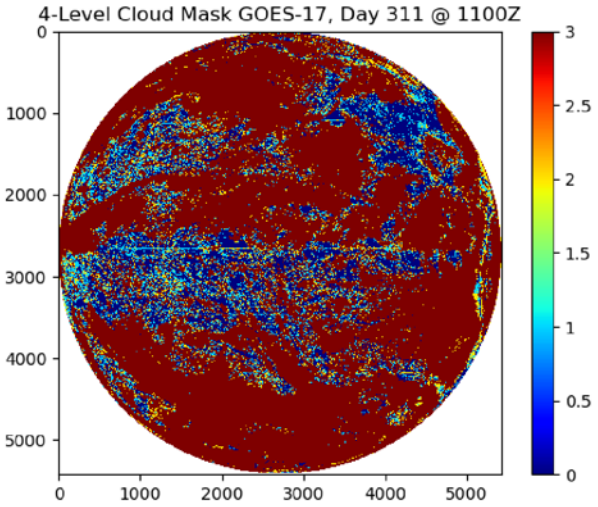

Figure 1. Cloud mask product during a GOES-17 LHP event

2.4.2 Cloud Phase and Type

The cloud type/phase routine is now part of the cloud mask algorithm, which replaces the previous standalone cloud type/phase algorithm. Similar to cloud probability, posterior ice/water cloud probability is computed from the retrieval algorithm. Based on the probability, the final cloud phase is classified into six categories, including clear, ice, water, supercooled, mixed, and unknown phases. Using additional tests in conjunction with the cloud phase, it also classifies each pixel into one of 11 categories: (0) clear, (1) probably clear, (2) fog, (3) liquid water, (4) supercooled water, (5) mixed, (6) opaque ice, (7) cirrus, (8) overlapping, (9) overshooting, (10) unknown. Additionally, if the retrieval uncertainty is large, cirrus cloud type is reclassified as overlapping cloud type, which is typically a semitransparent cirrus overlaying a warmer and lower-level cloud. Figure 2 shows that except for subvisible cirrus clouds that have very small optical depth, the CLAVR-x cloud phase compares well with CALIPSO and generally reaches the 80% specification requirement.

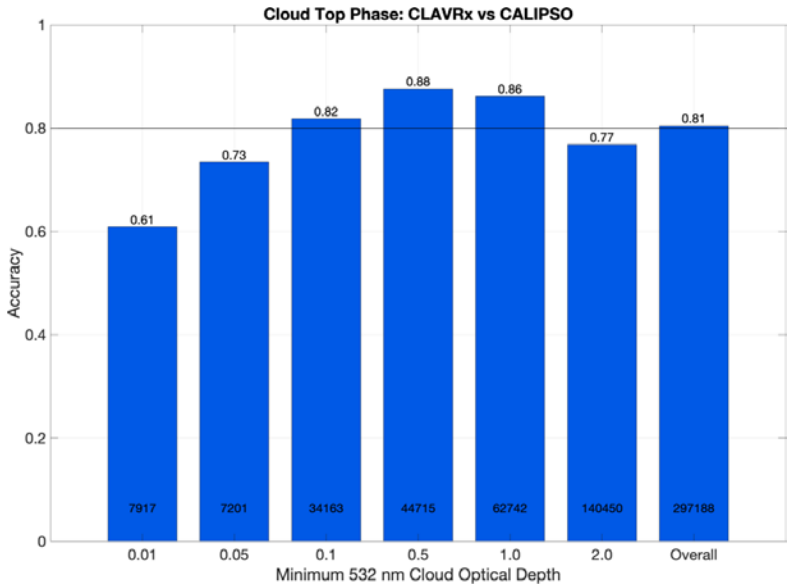

Figure 2. Validation of CLAVR-x cloud top phase using 9 days of matchup data between NOAA-21 and CALIPSO. This was taken from the NOAA-21 product review.

2.4.3 AWG Cloud Height Algorithm (ACHA)

ACHA is responsible for the estimation of the vertical cloud extent for all cloudy ABI pixels. It is directly responsible for the cloud top pressure, height, and temperature products. These products are also used to generate the cloud layer product that is being used by the aviation community to identify potential icing hazards. The ACHA results are currently used in the daytime and nighttime cloud optical and microphysical algorithms, the cloud base algorithm, and the Atmospheric Motion Vector (AMV) algorithm.

In general, ACHA relies on the infrared observations to avoid discontinuities associated with the transition from day to night. The ACHA performance is sensitive to imagery artifacts and instrument noise. Similar to the cloud mask algorithm, most important is our ability to accurately model the clear-sky values of the infrared absorption channels. The ability to perform the physical retrievals requires an accurate forward model, accurate ancillary data, and well-characterized spectral response functions. Infrared observations are impacted not only by the

height of the cloud but also its emissivity and how the emissivity varies with wavelength (a behavior that is tied to cloud microphysics). In addition, the emissions from the surface and the atmosphere can also be major contributors to the observed signal. Last, clouds often exhibit complex vertical structures that violate the assumptions of the single-layer plane parallel models (leading to erroneous retrievals). The job of the ACHA is to exploit as much of the information provided by the ABI as possible with appropriate, computationally efficient, and accurate methods to derive the various cloud height products.

The ACHA uses an analytical model of infrared radiative transfer embedded in an optimal estimation retrieval methodology. The optimal estimation approach, often referred to as a one-dimensional variational (1D-VAR), is described by Rodgers (1976). The benefits of this approach are that it is flexible and allows for the easy addition or subtraction of new observations or retrieved parameters. Another benefit of this approach is that it generates automatic estimates of the retrieval errors. The optimal estimation approach minimizes a cost function, Φ, given by:

$$\Phi = (x - x_a)^T S_a^{-1}(x - x_a) + \big(y - f(x)\big)^T S_y^{-1}\big(y - f(x)\big) \quad (2)$$

where **x** is a vector of the retrieved parameters, x_a is a vector housing the *a priori* values of **x** (which also serve as a first guess to begin iterations to a convergent solution), **y** is the vector of observations, and **f** is the forward model's estimates of the values of **y** under the assumptions of state **x**. $\mathbf{S_a}$ is the error covariance matrix corresponding to the values of x_a**,** and $\mathbf{S_y}$ is the error covariance matrix for the forward model and measurements.

ACHA combines multiple window channel observations with single absorption channel observations to allow for the estimation of cloud height without large assumptions on cloud microphysics. The actual channel set used in ACHA varies with sensor. ACHA provides many modes of operation depending on the availability of infrared channels. For GOES-R, the default ACHA modes use channels 14, 15 and 16 (11, 12 and 13.3 μm); however, modes that use channels 8, 9, 11 (6.2, 6.9, and 8.5 μm) are also supported. We assume the cloud microphysics and estimate cloud top temperature (CTT) and cloud emissivity (CEM). The choice for the assumed microphysical parameter has been guided by comparisons to MODIS CO_2 slicing results. The *a priori* constraints are based on the cloud type classification and MODIS CO_2 slicing results. For high, thin cirrus clouds, we have found CTT to be highly sensitive to the *a priori* constraint as well as CEM. The analysis has also demonstrated that the CTT accuracy allows for the proper placement of ice clouds in the high cloud category. For low-level clouds or optically thick high clouds, the method performs similarly to a single-channel 11-μm approach. This approach allows for the simultaneous estimation of CTT and CEM day and night. This algorithm is one reason that PATMOS-x high cloud amounts show realistic day-night differences. Subsequently, cloud top pressure and height are estimated from CTT using the collocated NWP atmospheric profile. Many types of NWP data are supported, and for ABI processing, the NCEP Climate Forecast System Reanalysis (CFSR) data are used.

In addition to the cloud height metrics (pressure/temperature/height) and cloud emissivity, the ACHA also provides an estimate of a microphysical parameter, β, derived from multiple emissivities that are related to particle size. Additionally, two other retrieval parameters are provided: the lower-level CTT under multilayer cloud conditions and the ice cloud fraction. These products are automatically generated by the ACHA and are useful for evaluating the ACHA's performance. Recent GOES-16, GOES-17, and GOES-18 ACHA product reviews have

shown that performance specification are met except for GOES-17 during the LHP event, and the mitigation approach is discussed next.

2.4.3.1 ACHA Mitigation for GOES-17 Loop Heat Pipe Issue

Two of the channels most affected (12.3 µm and 13.3 µm) during LHP events are used as input into the ACHA mode. This, in turn, degrades the quality of ACHA, and in the worst LHP events, no retrieval is made. Figure 3 shows the GOES-17 ACHA input channels for Aug. 30, 2019, at 1400 UTC during a severe LHP event.

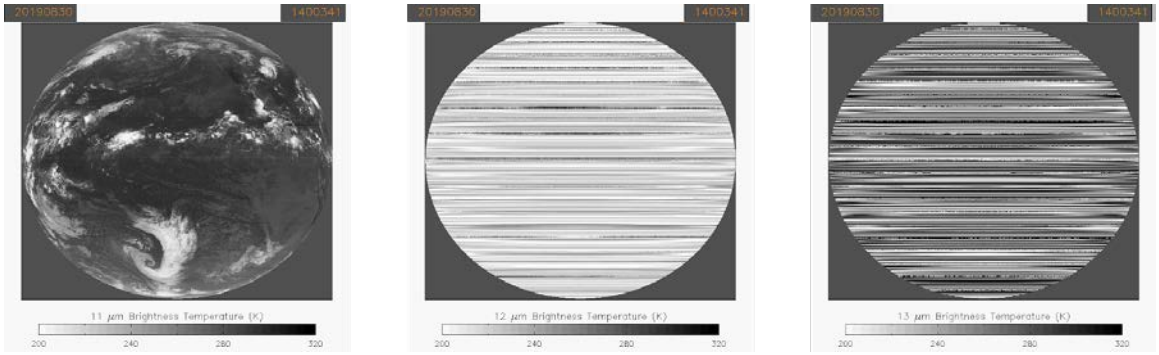

Figure 3. GOES-17 ACHA input channels on Aug. 30, 2019, at 1400 UTC. The 12.3-µm and 13.3-µm channels will cause the ACHA retrieval to fail.

The ABI detector cooling system is designed to run at a temperature of 81 K during normal heating days (June 15, 2019). During severe LHP events (Aug. 30, 2019), the temperature might rise to 107 K. This temperature is available in the Level 1b data as the variable "maximum_focal_plane_temperature". Tim Schmit (NOAA/NESDIS/Center for Satellite Applications and Research (STAR)) designed temperature thresholds for these LHP events, and NOAA Office of Satellite and Product Operations (OSPO) adopted these on Oct. 2, 2019 at 1704 UTC. CLAVR-x adopted the Warming Side Threshold, except for Band 14. This was kept at 100.0 K instead of 93.0 K.

During LHP events, the focal plane temperatures from the Level 1b data and the focal plane temperature thresholds are used to determine the "anchor channel" in ACHA. Within the CLAVR-x framework, a new module was created to check the thresholds and possibly turn channels off to upstream algorithms (mask, phase, ACHA) if the threshold values are exceeded. This module can set the 10.3-µm channel as the window channel, leave the 11.2-µm channel as the window, and possibly stop processing if both the 10.3-µm and 11.2-µm channels exceed their thresholds. If the 10.3-µm channel has been chosen, an internal flag is made available to ACHA.

For GOES-17, ACHA can modify the user-requested mode. During LHP events, the mode can change to one using the 3.9-µm and 11-µm channels or 3.9-µm and 10.3-µm channels. The call to ACHA first checks for the 10.3-µm use flag and will switch the following 11-µm channel variables to 10.3-µm values: (1) channel index, (2) 11-µm brightness temperatures, (3) 11-µm radiances, (4) 11-µm clear-sky radiances, (5) 11-µm surface emissivity, (6) 11-µm profiles of atmospheric radiances, (7) 11-µm profiles of atmospheric transmission, and (8) 11-µm black body radiance profiles. Note that this is a nighttime-only mode (~0830 UTC–1930 UTC).

2.4.4 Daytime Cloud Optical and Microphysical Properties (DCOMP)

The DCOMP algorithm is responsible for generating the cloud optical depth (COD) and cloud particle size (CPS) products for all daytime ABI pixels that are detected as cloudy. Subsequently, liquid water path (LWP) and ice water path (IWP) products are derived from COD and CPS. COD represents the vertical optical thickness between the top and bottom of an atmospheric column. COD is almost independent of wavelength in the visible range of the spectrum and has no unit. CPS is supposed to represent the cloud droplet size distribution. The effective cloud particle radius (CRE), defined as the ratio of the third to the second moment of a droplet size distribution, is well suited to fulfill this task. CRE has the unit micrometer (μm). LWP and IWP are a measure of the total mass of water in a cloud column. The unit is gram per square meter (g/m^2). In our context, *daytime* is defined to be when the solar zenith angle for a given pixel is less than or equal to 65 degrees, for which DCOMP provides full quality products; however, to fill a temporal gap between DCOMP and the nighttime cloud properties algorithm, degraded products for solar zenith angles between 65 and 82 degrees are provided by DCOMP.

DCOMP was developed at CIMSS and is described in Walther and Heidinger (2012).

DCOMP is based on earlier methods that also retrieve COD and CRE from visible and near-infrared wavelengths (King 1987; Nakajima and King 1990; Nakajima and King 1992). To briefly describe the underlying idea of the retrieval, COD, referred to as absorption-free wavelengths (for instance to 550 nm), is determined by the amount of light scattering by cloud droplets. The size of the droplets is responsible for absorption and the transition to a new direction of scattered photons, expressed by the phase function, $P(\theta)$, which is a function of the scattering angle, θ. Because CRE is a measure of the volume of cloud particles, it is mirrored in the absorption amount of clouds. The basic premise is that COD and CRE are inferred from solving the radiative transfer equation for a single-layer, plan-parallel, homogeneously distributed cloud above a Lambertian surface. The retrieval concept is based on a 1D radiation concept where a cloud completely covers a pixel. For DCOMP, the COD and CRE are retrieved for daytime observations by an optimal estimation approach using 0.6 μm and one near-infrared channel, such as 3.75 μm (Walther and Heidinger 2012). The forward operator is based on Mie theory and an adding/doubling RTM. For ice phase functions, we use ice crystal habit distributions as described by Baum et al. (2005). The forward simulation output is stored in LUTs to speed up the retrieval. The surface reflectance over land for 0.63 μm is taken from white-sky albedo maps generated by the MODIS-ST group. The 3.75-μm surface reflectance and emissivity over land is provided by the SEEBOR emissivity database (Seemann et al. 2008). Over ocean, fixed values of surface reflectance and emissivity are assumed. Because DCOMP needs two channels, one of visible spectrum at 0.6 μm, we defined DCOMP processing modes 1, 2, and 3, which are associated with 1.6 μm, 2.25 μm, and 3.75 μm, respectively. In addition, DCOMP mode 9 processes all modes (1, 2, 3) and writes all modes output in a Level 2 file.

Knowing a measure of the size distribution with CPS and a measure of the vertical thickness of a cloud column given by COD also enables retrievals, under certain assumptions, of the amount of water within the cloud. We separate this value into the LWP and IWP to correspond with the dominant water phase in the cloud. We derive the LWP and IWP using COD and CRE by $LWP = 5/9 * COD * CRE$ for liquid cloud phase (Wood and Hartmann 2006) and $IWP = [COD^{(1/0.84)}]/0.065$ for IWP (Heymsfield et al. 2003). The Heymsfield relationship was derived empirically from aircraft measurements. The motivation for this choice is that the cloud top

effective radius for thick ice clouds has little correlation with the effective radius deeper in the cloud. Our analysis indicates that this empirical relationship based solely on COD gives values higher than those predicted by the method employed for water clouds.

Generally, the retrieval strategy in DCOMP includes the following:

- Apply an RTM to quantify the influence of the cloud microphysical parameters on the backscattered solar radiation measured at the sensor.
- Generate LUTs for cloud reflectivity, cloud transmission, spherical albedo, and cloud albedo of one channel in the visible spectrum at 0.6 μm and for one near-infrared channel at either 1.6 μm, 2.2 μm, or 3.75 μm with respect to DCOMP mode from 1 to 3 for a wide range of possible sun/sensor geometry constellations.
- Receive from the processing framework all other cloud-related derived products (cloud mask, cloud height, and cloud phase) and ancillary data needed by the COD/CRE algorithms.
- Use 1D-VAR optimal estimation inversion techniques to retrieve the optical thickness and particle size from the LUTs of channel reflectivity based on the optimal estimation method.

DCOMP does not directly suffer from LHP events but will be impacted by upstream products, including cloud mask, phase, and ACHA. Table 1 shows the validation of the GOES-17 ABI DCOMP products against NASA MODIS, and the performance generally meets the specifications.

Table 1. Validation of GOES-17 DCOMP Products Against NASA MODIS

Parameter	Specified Measurement Accuracy (COD > 1)	Observed Accuracy	Specification (%)
COD water	20%	16%	43.3
COD ice	30%	19%	54.6
CRE water	4 μm	6.4 μm	75
CRE ice	10 μm	2.5 μm	58

References

Baum, B. A., A. J. Heymsfield, P. Yang, and S. T. Bedka. 2005. "Bulk Scattering Properties for the Remote Sensing of Ice Clouds. Part I: Microphysical Data and Models." *Journal of Applied Meteorology and Climatology* 44: 1,885–1,895.

CLAVR-x user guide, accessible from https://docs.google.com/document/d/1NHuKBJr23i1k0ysihoyThg32e44l4CoDe5CjWydn0JI/edit .

Dybbroe, A., K. G. Karlsson, and A. Thoss. 2005a. "NWCSAF AVHRR Cloud Detection and Analysis Using Dynamic Thresholds and Radiative Transfer Modeling. Part I: Algorithm Description." *Journal of Applied Meteorology and Climatology* 44: 39–54.

Dybbroe, A., K. G. Karlsson, and A. Thoss. 2005b. "NWCSAF AVHRR Cloud Detection and Analysis Using Dynamic Thresholds and Radiative Transfer Modeling. Part II: Tuning and Validation." *Journal of Applied Meteorology and Climatology* 44: 55–71.

GOES-R ABI Cloud Height Algorithm Theoretical Basis Document, accessible from https://www.star.nesdis.noaa.gov/goesr/documents/ATBDs/Enterprise/ATBD_Enterprise_Cloud_Height_v3.4_2020-09.pdf

GOES-R ABI Cloud Mask Algorithm Theoretical Basis Document, accessible from https://www.star.nesdis.noaa.gov/goesr/documents/ATBDs/Enterprise/ATBD_Enterprise_Cloud_Mask_v1.2_2020_10_01.pdf

GOES-R ABI Daytime Cloud Optical and Microphysical Properties (DCOMP) Algorithm Theoretical Basis Document, accessible from https://www.star.nesdis.noaa.gov/goesr/documents/ATBDs/Enterprise/ATBD_Enterprise_Daytime_Cloud_Optical_and_Microphysical_Properties(DCOMP)_v1.2_2020-10-09.pdf

GOES-R Level 1 Requirements Document (L1RD), accessible from https://www.goes-r.gov/syseng/docs/LIRD.pdf

GOES-R Series Ground Segment (GS) Project Functional and Performance Specification (F&PS) [G416-R-FPS-0089], accessible from https://www.goes-r.gov/resources/docs/GOES-R_GS_FPS.pdf

GOES-R Series Mission Requirements Document (MRD) [410-R-MRD-0070], accessible from https://www.goes-r.gov/syseng/docs/MRD.pdf

Heidinger, A. K., and M. J. Pavolonis. 2009. "Gazing at Cirrus Clouds for 25 Years Through a Split Window, Part I: Methodology." *Journal of Applied Meteorology and Climatology* 48 (6): 1,100–1,116.

Heymsfield. 2003. "Ice Water Path-Optical Relationships for Cirrus and Deep Stratiform Ice Cloud Layers." *Journal of Applied Meteorology and Climatology* 42 (10): 1,369–1,390.

King, M. D. 1987. "Determination of the Scaled Optical-Thickness of Clouds From Reflected Solar-Radiation Measurements." *Journal of the Atmospheric Sciences* 44 (13): 1,734–1,751.

Nakajima, T., and M. D. King. 1990. "Determination of the Optical-Thickness and Effective Particle Radius of Clouds From Reflected Solar-Radiation Measurements. Part 1: Theory. *Journal of the Atmospheric Sciences* 47 (15): 1,878–1,893.

Nakajima, T., and M. D. King. 1992. "Asymptotic Theory for Optically Thick Layers—Application to the Discrete Ordinates Method." *Applied Optics* 31 (36): 7,669–7,683.

Rodgers, C. D. 1976. "Retrieval of Atmospheric Temperature and Composition From Remote Measurements of Thermal Radiation." *Reviews of Geophysics* 60: 609–624.

Seemann, S. W., E. E. Borbas, R. O. Knuteson, G. R. Stephenson, and H.-L. Huang. 2008. "Development of a Global Infrared Land Surface Emissivity Database for Application to Clear-Sky Sounding Retrievals From Multi-Spectral Satellite Radiance Measurements*." Journal of Applied Meteorology and Climatology* 47 (1): 108–123.

STAR JPSS Enterprise Cloud Mask Algorithm Theoretical Basis Document, accessible from https://docs.google.com/document/d/18e67VUspdlTY_pn5mBYrTHSJDew0d2nmk8BylijuK9s/edit

STAR JPSS Enterprise Cloud Height Algorithm Theoretical Basis Document, accessible from https://docs.google.com/document/d/1m2SatR91WIJcaAZweongcFCb6Wsx_xnRUcZxp94gXHk/edit

Walther, A., and A. K. Heidinger. 2012. "Implementation of the Daytime Cloud Optical and Microphysical Properties algorithm (DCOMP) in PATMOS-x." *Journal of Applied Meteorology and Climatology* 51 (7): 1,371–1,390.

Wood, R., and D. L. Hartmann. 2006. "Spatial Variability of Liquid Water Path in Marine Low Cloud: The Importance of Mesoscale Cellular Convection." *Journal of Climate* 19: 1,748–1,764.

Appendix A

Table A-1. Description of the Level 2 Output Variables

The contents of any given Level 2 file are controlled by the variables in the level2_list file. The assumed missing value is -999. For unscaled variables, the Range_Min and Range_Max are set to missing.

Name	Units	Range Min	Range Max	Long Name
longitude	degrees_east	-180.0	180.0	Longitude
latitude	degrees_north	-90.0	90.0	Latitude
scan_line_time	Hours	0.0	24.0	Time for the scan line in fractional hours
scan_line_number	None	1	Varies	Scan line number
bad_scan_line_flag	None	0	1	Flag to indicate if a scan line is bad
bad_pixel_mask	None	0	1	Mask that distinguishes good (0) from bad (1) pixels
latitude_pc	degrees_north	-90.0	90.0	latitude_parallax_corrected_using_cloud_height
longitude_pc	degrees_east	-180.0	180.0	longitude_parallax_corrected_using_cloud_height
sensor_zenith_angle	Degrees	0.00	90.0	Sensor zenith for each pixel measured in degrees from nadir
solar_zenith_angle	Degrees	0.00	180.0	Solar zenith for each pixel measured in degrees away from the sun (0 = looking at sun)
relative_azimuth_angle	Degrees	0.00	180.0	Relative azimuth angle in degrees; 0 is the principal plane looking toward sun
solar_azimuth_angle	Degrees	-180.0	180.0	Solar azimuth angle in degrees from north, pixel to sun; positive values are clockwise from north
sensor_azimuth_angle	Degrees	-180.0	180.0	Sensor azimuth angle in degrees from north, pixel to sensor; positive values are clockwise from north
glint_mask	None	0	1	Glint mask (0 = no) (1 = yes)
coast_mask	None	0	1	Coast mask (0 = no) (1 = yes)

Name	Units	Range Min	Range Max	Long Name
surface_type	None	0	13	UMD surface type: • water = 0 • evergreen_needle = 1 • evergreen_broad = 2 • deciduous_needle = 3 • deciduous_broad = 4 • mixed_forest = 5 • woodlands = 6 • wooded_grass = 7 • closed_shrubs = 8 • open_shrubs = 9 • grasses = 10 • croplands = 11 • bare = 12 • urban = 13
land_class	None	0	7	Land classes and values: • shallow ocean = 0 • land = 1 • coastline = 2 • shallow inland water = 3 • ephemeral water = 4 • deep inland water = 5 • moderate ocean = 6 • deep ocean = 7
snow_class	None	0	3	Snow classes and values: • no snow/ice = 1 • sea_ice = 2 • snow = 3
scattering_angle	Degrees	0.00	180.0	Angle for each pixel measured in degrees away from direction of forward scattering
surface_elevation	Meters	-500.0	10000.0	Surface elevation above mean sea level
refl_0_65um_nom	%	-2.00	120.0	Top of atmosphere reflectance at the nominal wavelength of 0.65 microns
refl_0_86um_nom	%	-2.00	120.0	Top of atmosphere reflectance at the nominal wavelength of 0.86 microns
refl_1_60um_nom	%	-2.00	120.0	Top of atmosphere reflectance at the nominal wavelength of 1.60 microns

Name	Units	Range Min	Range Max	Long Name
refl_3_75um_nom	%	-20.0	80.0	Top of atmosphere reflectance at the nominal wavelength of 3.75 microns
temp_3_75um_nom	K	180.0	340.0	Top of atmosphere brightness temperature at the nominal wavelength of 3.75 microns
temp_11_0um_nom	K	180.0	340.0	Top of atmosphere brightness temperature at the nominal wavelength of 11.0 microns
temp_12_0um_nom	K	180.0	340.0	Top of atmosphere brightness temperature at the nominal wavelength of 12.0 microns
refl_0_65um_nom_ stddev_3x3	%	0.00	20.0	Standard deviation of the 0.63-micron reflectance computed over a 3 x 3 pixel array
temp_11_0um_nom_ stddev_3x3	K	0.00	20.0	Standard deviation of the 11-micron brightness temperature computed over a 3 x 3 pixel array
cloud_probability	None	0.00	1.00	Probability of a pixel being cloudy from the Bayesian cloud mask
cloud_mask	None	0.00	3	Integer classification of the cloud mask, including: • clear = 0 • probably clear = 1 • probably cloudy = 2 • cloudy = 3

Name	Units	Range Min	Range Max	Long Name
cloud_type	None	0	13	Integer classification of the cloud type including clear and aerosol type: • 0 = clear • 1 = probably clear • 2 = fog • 3 = water • 4 = supercooled water • 5 = mixed • 6 = opaque_ice • 7 = cirrus • 8 = overlapping • 9 = overshooting • 10 = unknown • 11 = dust • 12 = smoke • 13 = fire
cloud_phase	None	0	5	Integer classification of the cloud phase including clear and aerosol type: • 0 = clear • 1 = water • 2 = supercooled water • 3 = mixed • 4 = ice • 5 = unknown
cld_press_acha	hPa	0.00	1100.00	Cloud top pressure computed using the ACHA
cld_temp_acha	K	180.0	320.0	CTT computed using the ACHA
cld_height_acha	km	0.00	20.0	Cloud height computed using the ACHA
cld_emiss_acha	None	0.00	1.00	Cloud emissivity at the nominal wavelength of 11 microns, determined from the ACHA
cld_opd_dcomp	None	-0.2	160.0	COD at the nominal wavelength of 0.65 microns, determined from DCOMP
cld_reff_dcomp	Micron	0.00	160.0	Effective radius of cloud particles determined from DCOMP; see attributes for channels used

Name	Units	Range Min	Range Max	Long Name
dcomp_quality	None	0.00	1	Quality flags for DCOMP products in bits; 1. Processed (0 = no,1 = yes) 2. Valid COD retrieval (0 = yes,1 = no) 3. Valid CRE retrieval (0 = yes,1 = no) 4. Degraded COD retrieval (0 = no,1 = degraded) 5. Degraded CRE retrieval (0 = no,1 = degraded) 6. Convergency (0 = no,1 = yes) 7. Flint
surface_temperature_retrieved	K	220	340	Retrieved surface temperature
cloud_fraction	None	0	1.0	Total cloud fraction from cloud cover layer algorithm
cloud_albedo_0_65um_nom	None	0	1.0	Cloud albedo at the nominal wavelength of 0.65 micron from DCOMP
cloud_transmission_0_65um_nom	None	0	1.0	Cloud transmission at the nominal wavelength of 0.65 micron
temp_6_7um_nom	K	180.0	340.0	Top of atmosphere brightness temperature at the nominal wavelength of 6.7 microns
temp_7_3um_nom	K	180.0	340.0	Top of atmosphere brightness temperature at the nominal wavelength of 7.3 microns
temp_8_5um_nom	K	180.0	340.0	Top of atmosphere brightness temperature at the nominal wavelength of 8.5 microns
temp_9_7um_nom	K	180.0	340.0	Top of atmosphere brightness temperature at the nominal wavelength of 9.7 microns
temp_13_3um_nom	K	180.0	340.0	Top of atmosphere brightness temperature at the nominal wavelength of 13.3 microns
refl_0_47um_nom	%	-2.00	120.0	Top of atmosphere reflectance at the nominal wavelength of 0.47 microns
Refl_0_65um_nom_min_sub	%	-2.00	120.0	Minimum of the 0.63 micron reflectance read from the high resolution data

Name	Units	Range Min	Range Max	Long Name
Refl_0_65um_nom_ max_sub	%	-2.00	120.0	Maximum of the 0.63 micron reflectance read from the high resolution data
refl_1_38um_nom	%	-2.00	120.0	Top of atmosphere reflectance at the nominal wavelength of 1.38 microns

Appendix B

The following figures show examples of previous GOES PATMOS-x cloud products.

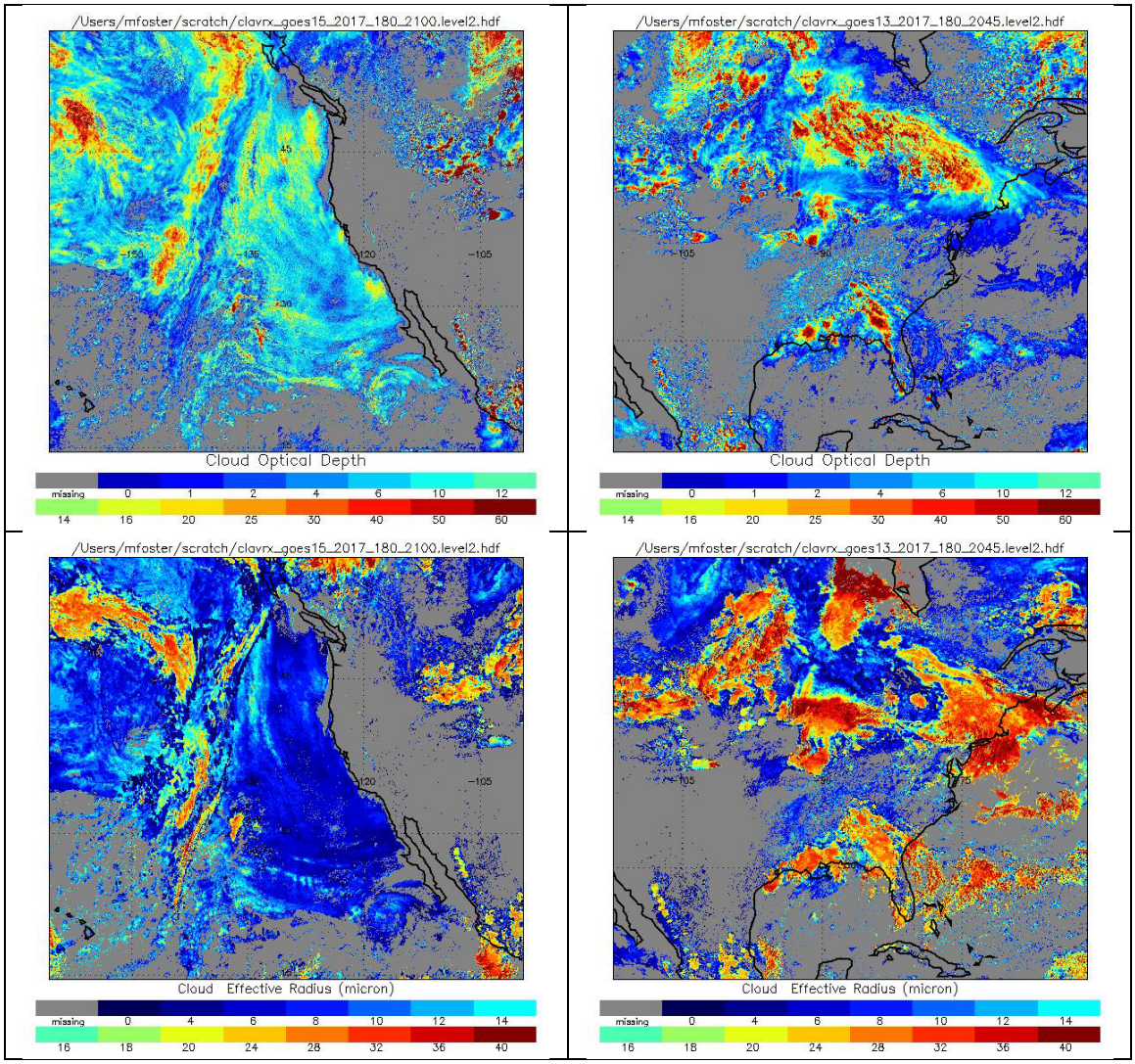

Figure B-1. Cloud optical depth and effective particle size retrieved at a 15-minute interval from GOES-13 (East) and GOES-15 (West) late afternoon on June 29, 2017

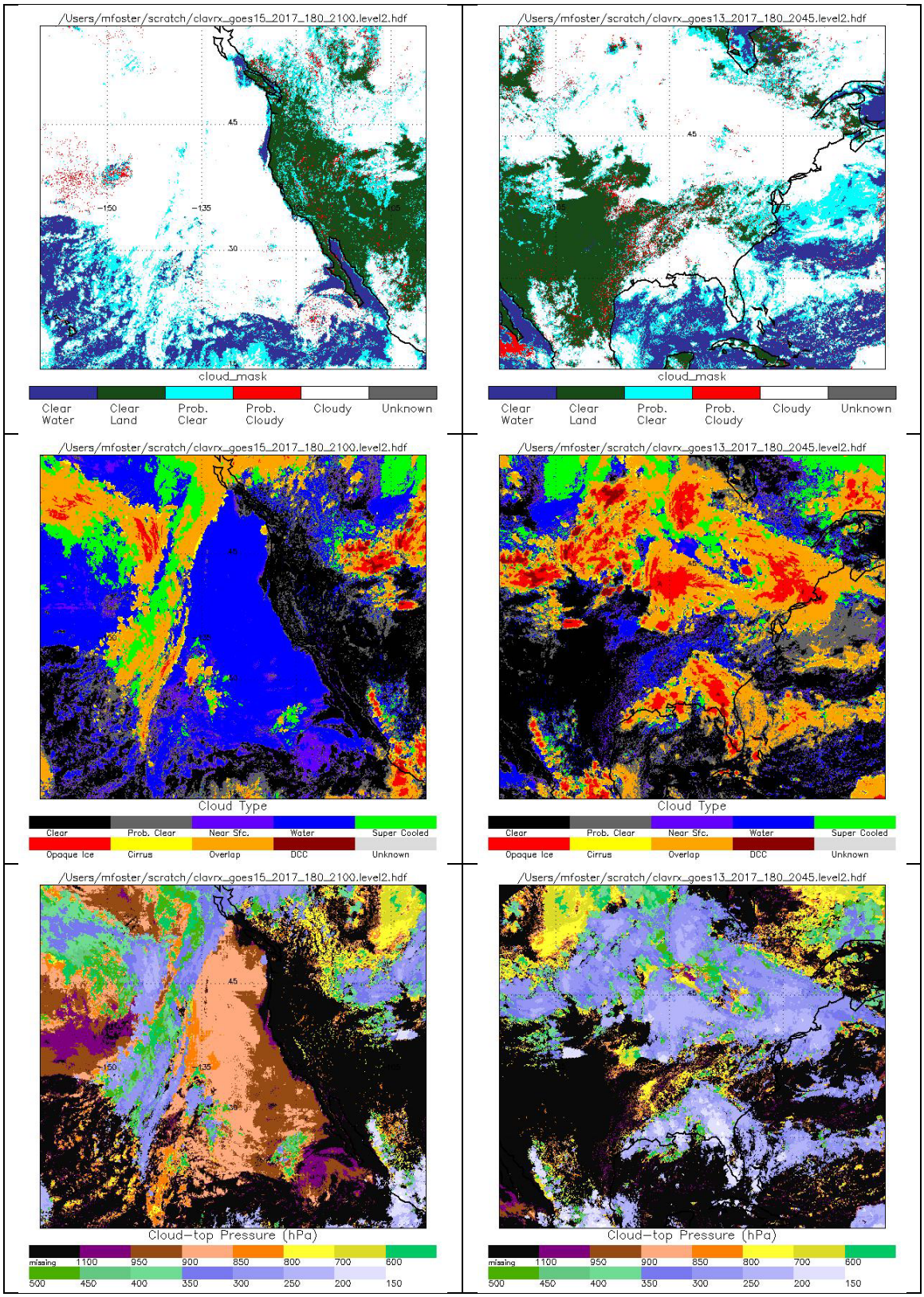

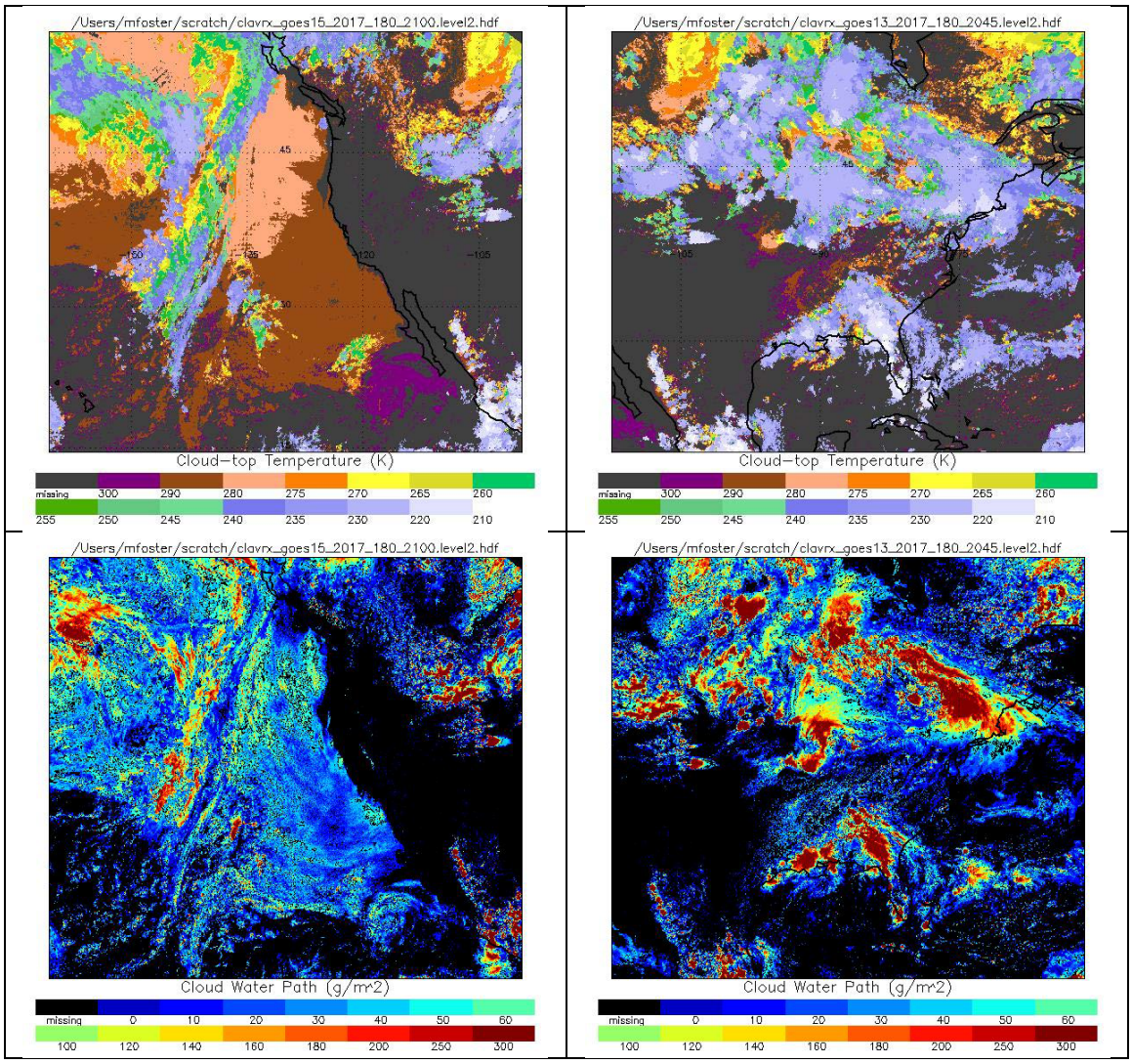

Figure B-2. Cloud mask, type, cloud top, and water path retrieved at a 15-minute interval from GOES-13 (East) and GOES-15 (West) late afternoon on June 29, 2017

The following figures show examples of the same products for the GOES-R series full disk products over the contiguous United States. The left shows the example for GOES-16, and the right shows the example for GOES-18. The retrieval products from the two sensors agree well. The larger differences in effective particle size are seen over eastern contiguous United States, which are likely caused by a large satellite zenith angle in GOES-18.

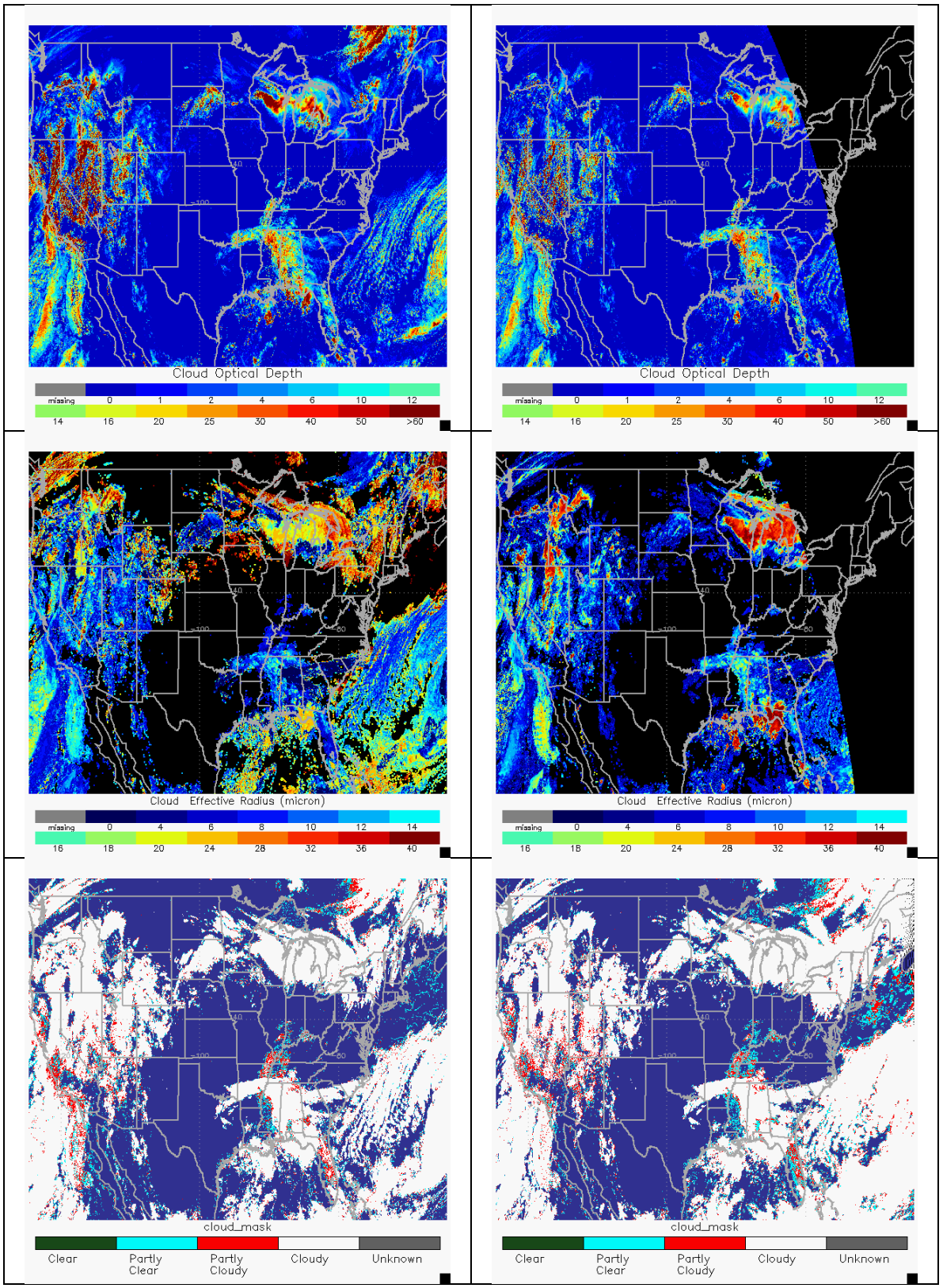

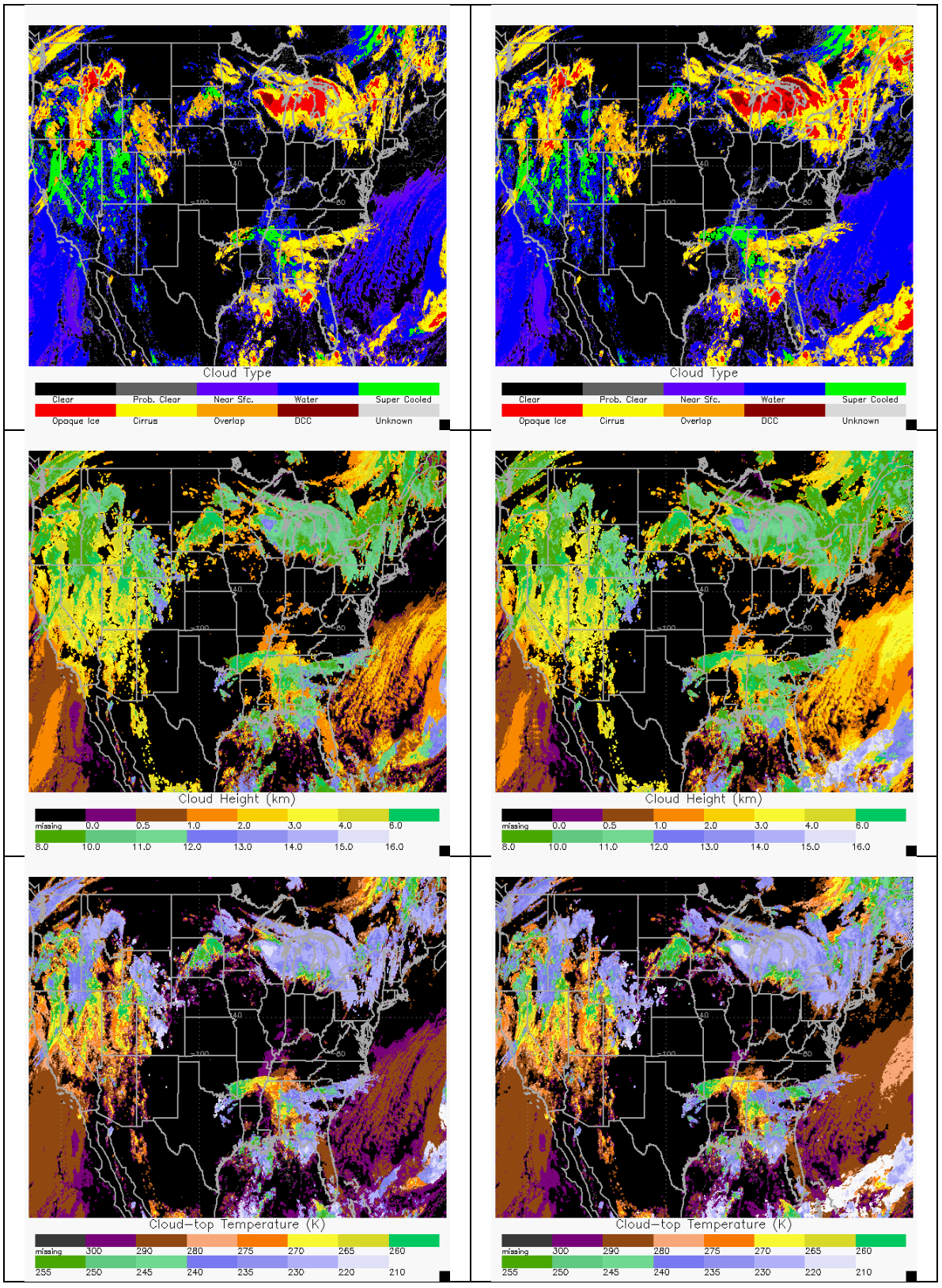

Figure B-3. Cloud optical depth, effective particle size, mask, type, and cloud top information retrieved from GOES-16 (East) and GOES-18 (West) at 1530 UTC on Sept. 2, 2023.